Chemical Engineering Journal 101 (2004) 391–396

Chemical Engineering Journal

www.elsevier.com/locate/cej

A model for predicting axial mixing during gas–liquid Taylor flow in microchannels at low Bodenstein numbers

Wael Salman, Asterios Gavriilidis, Panagiota Angeli*

Department of Chemical Engineering, University College London, Torrington Place, London WC1E 7JE, UK

Received 31 July 2003; accepted 13 October 2003

Abstract

A numerical model has been developed for the study of axial mass transfer in gas–liquid Taylor flow at low Bodenstein numbers. The model assumes well mixed liquid slugs of uniform concentration and liquid films around the bubbles that can be adequately described by a one-dimensional convection-diffusion equation. A finite volume method was used for its solution. It was found that the model is suitable for $Ca < 10^{-3}$, $Bo < 500$ and $L_s < 16$. In addition for $Bo > 10$ it could be approximated by a simple analytical expression.

The results showed that axial mixing is low and increases with increasing film thickness as well as increasing bubble and slug lengths.

Keywords: Two phase; Taylor flow; Axial mixing; Low Bodenstein number

1. Introduction

Taylor flow is one of the dominant two phase flow patterns in microscale diameter channels. It consists of elongated bubbles of equivalent diameter larger than the tube diameter separated by liquid slugs. The bubbles adopt a characteristic capsular shape. They completely fill the channel cross section and are only separated from the wall by a thin film of liquid. Because of the presence of bubbles in front and at the back of the slugs, the flow field in the liquid is modified compared to single phase flow, and toroidal vortices are formed [1].

Compared to single-phase laminar flow, Taylor flow offers many advantages [2]. These can be summed up as follows:

(1) The recirculation within the liquid slugs improves radial mass transfer, i.e. from liquid to wall and from gas to liquid [3–5].
(2) The separation of the bulk liquid with the bubbles significantly reduces axial mixing between liquid slugs. The film surrounding the bubbles is the only means of communication between two successive slugs and in the majority of cases its thickness is only a fraction of a percentage of the tube diameter.

The combination of good radial mass transfer and low axial mass transfer in the liquid makes Taylor flow suitable for two-phase applications that involve mass transfer (fluid–fluid or wall-fluid) or single phase liquid applications which suffer from large backmixing. The latter can be significant in microscale systems where low sample volumes are involved. Taylor flow has also been suggested as a means of introducing sequentially different reactants/samples within a microchannel reactor/analyser to avoid their mixing [6]. Although Taylor flow significantly reduces axial mixing, it does not eliminate it, because of the liquid film around the bubbles that connects the slugs. In high throughput experimentation systems it becomes important to be able to quantify axial mixing so that sufficient time/separation between the injected samples is introduced.

Existing axial mixing studies during Taylor flow in microchannels originate mainly from two-phase catalytic monolith applications [2,7,8]. Pedersen and Hovarth [9] proposed a model for axial mass transfer in capillaries with Taylor flow where the liquid slug was divided into two separate regions, the first containing the recirculating liquid and the second consisting of the liquid film flowing between the slugs. Perfect mixing was assumed in the two regions and the mass transfer between them was controlled by an adjustable parameter. Thulasidas et al. [8] also divided the liquid slug into two separate well mixed regions, namely, a recirculating slug and a film, that exchange mass by diffusion only. Their model had no adjustable parameters and reasonably matched experimental results on residence time

* Corresponding author. Tel.: +44-207-679-3832; fax: +44-207-383-2348.
E-mail address: p.angeli@ucl.ac.uk (P. Angeli).

1385-8947/$ – see front matter © 2004 Elsevier B.V. All rights reserved.
doi:10.1016/j.cej.2003.10.027

Nomenclature

A	cross sectional area of film (m^2)
Bo	Bodenstein number ($U_b d/D$)
Ca	capillary number ($\mu U_b/\gamma$)
d	microchannel diameter (m)
D	diffusivity of tracer species (m^2/s)
D_e	dispersion coefficient (m^2/s)
$E(t)$	residence time distribution curve
Fr	Froude number (U_b^2/gd))
g	acceleration due to gravity (m/s^2)
k	tracer cell number
L_s	slug length (m)
L_b	bubble length (m)
L_{cell}	cell length (m)
$L_{reactor}$	reactor length (m)
N	total number of cells in model
N_A	number of cells ahead of tracer cell
N^i	flux (kg/m^2 s)
Re	Reynolds number ($\rho U_b d/\mu$)
t	time (s)
t_m	mean of RTD (s)
$\boldsymbol{u}$	velocity field in liquid slug (m/s)
u	one dimensional liquid velocity (m/s)
U_b	bubble velocity (m/s)
V	volume of a liquid slug (m^3)
VDN	vessel dispersion number ($D_e/U_b L_{reactor}$)
x	axial coordinate (m)

Greek symbols

γ	interfacial tension (N/m)
δ	thickness of film surrounding bubble (m)
μ	liquid viscosity (Ns/m^2)
ρ	density (kg/m^3)
σ	standard deviation of RTD (s)
τ_p	residence time for PFR (s)
τ_s	residence time for CSTR (s)

Superscripts

i	species number
$+$	left end of the liquid slug
$-$	right end of the liquid slug
$\bar{x}$	barred symbols are non-dimensionalised

Subscripts

0	initial value at $t = 0$

distribution in single channels obtained by the authors. The regions close to the bubbles and the convection-diffusion taking place in them were however neglected because of the long slugs assumed. For short slugs, of the order of a few channel diameters, these regions have considerable effect on the overall mass transfer. In addition, for low Bodenstein number (Bo) values the diffusing species is stripped from the thin film at the leading end of the liquid slug, and the assumption of two separate well mixed regions fails.

The present work is aimed at the study of axial mixing at low Bodenstein numbers where slugs are assumed well mixed and a unidirectional convection-diffusion equation can describe mass transfer in the liquid film surrounding the bubbles. The applicability of the model is also assessed for a range of system parameters.

2. Model development

The parameters that are expected to affect axial mixing in Taylor flow are the thickness of the liquid films that surround gas bubbles, the length of the bubbles, which determines the length of the liquid films, and the length of the liquid slugs which affects recirculation and mass transfer within these slugs. The film thickness depends on the balance of inertial, viscous and gravitational forces in the liquid and the surface tension force along the interface, or on the following dimensionless numbers [10]: capillary number (*Ca*), Reynolds number (*Re*) and Froude number (*Fr*). The influence of the two numbers *Re* and *Fr* decreases with decreasing *Ca* values and for $Ca < 10^{-3}$ the film thickness can be correlated only to *Ca*. Different correlations (summarised by Edvinsson and Irandoust [10]) derived from experimental studies relate film thickness to *Ca*.

For given gas and liquid flow rates, different combinations of bubble and slug lengths can satisfy the overall mass balance [11]. In capillaries where surface tension dominates, bubble breakup and coalescence within the channel are absent, and bubble and slug sizes will be determined by the conditions at the channel inlet, where the two phases meet. Different geometries and flowrates will affect both lengths. It is possible, therefore to produce the required bubble and slug lengths by varying the inlet channel geometry. Based on this, the current study is not concerned with bubble formation at the channel inlet but assumes that certain repeating (constant) bubble and slug lengths exist within the microchannel. In the analysis below a single unit of the repeating pattern comprising a single bubble and a single slug, or a slug and two half bubbles is called a “unit cell”, (see Fig. 1).

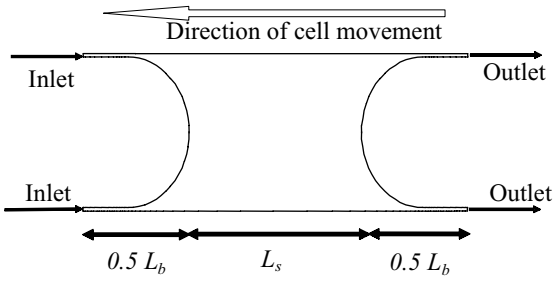

Fig. 1. Schematic of a unit cell with two half bubbles and one liquid slug. The length of the bubble is L_b. The length of the slug is L_s.

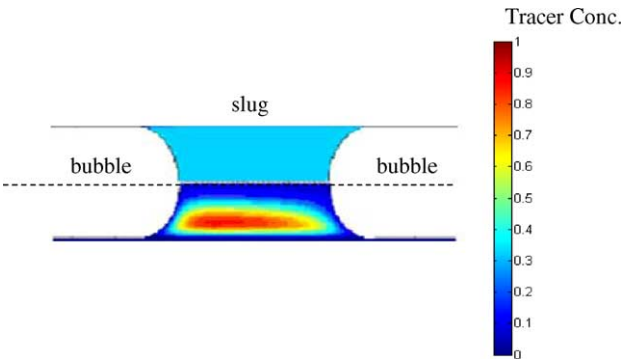

Fig. 2. Tracer concentration in a liquid slug with initial unit concentration after it passed through a reactor ($\bar{L}_{\text{reactor}} = 333$)filled with tracer free liquid. Top: $Bo = 990$, Bottom: $Bo = 64{,}800$.

To study axial mixing a pulse of tracer is added as a unit cell of concentration ρ_0 in the microchannel at time $t = 0$. The concentrations in the slugs exiting the reactor give the residence time distribution curve. All other unit cells ahead and behind the tracer cell have initially 0 concentration. As the tracer unit cell moves in the reactor some tracer is transferred from it to the neighbouring cells through the liquid film. In a moving frame of reference with the same velocity as the initial tracer cell, each unit cell resembles a vessel with an inlet and an outlet (see Fig. 1).

The convection-diffusion equation can be written in dimensionless form for a unit cell as follows:

$$\frac{\partial \bar{\rho}^i}{\partial \bar{t}} + \bar{\boldsymbol{u}}\,\bar{\nabla}\bar{\rho}^i - \left(\frac{1}{Bo}\right)\bar{\nabla}^2\bar{\rho}^i = 0 \tag{1}$$

where all terms have been appropriately non-dimensionalised.

To solve Eq. (1) the flow field $\bar{\boldsymbol{u}}$ in the convection term needs to be known. With decreasing Bodenstein number, the diffusion term in the equation starts to gain importance. The increased importance of diffusion coupled with recirculation means that concentration within the slugs becomes uniform very quickly [12], (see Fig. 2). The increased importance of diffusion however, can also result in a flux of the tracer from both ends of the unit cell. To account for this, the cells both in front and at the back of the tracer injection cell need to be taken into account. Each of the surrounding cells will also have a tracer concentration that will be linked via the film to the cells surrounding it and so on. It is therefore important to include in the modeling a sufficient number of cells on both sides of the initial tracer cell so that the end cells on either side have negligible tracer concentrations and there is no mass transfer between them and their neighbours. At the boundaries of the first and last cells, tracer flux can then be neglected. It is also assumed that the film surrounding the bubbles has uniform velocity and is well mixed radially. As a result the film can be adequately modelled using a unidirectional convection-diffusion equation. A schematic diagram of the elements used in the model is shown in Fig. 3.

The following characteristic parameters are used to non-dimensionalise Eq. (1).

Characteristic time	$\dfrac{d}{U_\text{b}}$
Characteristic length	d
Characteristic velocity	U_b

The characteristic time is related to convection which will still dominate even at increased diffusion contribution.

For the analysis of axial mixing with a step or pulse change, the following transform is applied

$$\rho^{-i} = \frac{\rho^i}{\rho_0^i}$$

where ρ_0^i is the tracer concentration in the tracer unit cell at time t_0 and i refers to the tracer species.

For any film k the resulting equation can be stated as:

$$\left\{\frac{\partial \bar{\rho}^i}{\partial \bar{t}} + \left(\frac{\partial \bar{\rho}^i}{\partial \bar{x}}\right) - \frac{1}{Bo}\frac{\partial^2 \bar{\rho}^i}{\partial \bar{x}^2}\right\}_k = 0 \tag{2}$$

For a mixed slug region k of volume V and a film having a cross-sectional area A (see Fig. 4), a mass balance yields:

$$\left\{V\frac{\partial \rho^i}{\partial t} + A(N^{i-} - N^{i+})\right\}_k = 0 \tag{3}$$

where N^{i-} and N^{i+} refer to the fluxes downstream and upstream of the slug, respectively, that can be found from

$$N^{i-} = \left\{(u\rho^i) - D^i\frac{\partial \rho^i}{\partial x}\right\}_{x^-} \tag{4}$$

$$N^{i+} = \left\{(u\rho^i) - D^i\frac{\partial \rho^i}{\partial x}\right\}_{x^+} \tag{5}$$

Points x^- and x^+ refer to the positions at the left and right ends of the liquid slug.

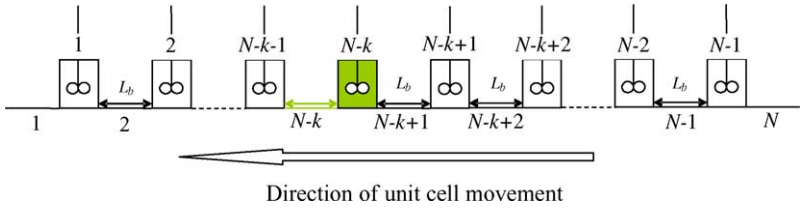

Fig. 3. Schematic diagram of the elements of the model. The tracer is initially introduced in a single unit cell at position k with $N - k + 1$ cells behind and $k - 1$ cells in front.

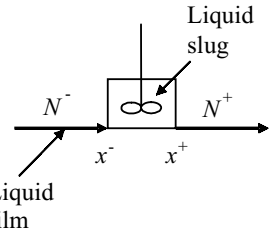

Fig. 4. Diagram depicting the mass balance on a single slug. The volume of the liquid slug is V and the tracer flux into the volume is through a film of cross sectional area A.

Eqs. (3)–(5) can be non-dimensionalised to give

$$\left\{\frac{\bar{V}}{\bar{A}}\frac{\partial\bar{\rho}^i}{\partial\bar{t}} + (\bar{N}^{i-} - \bar{N}^{i+})\right\}_k = 0 \tag{6}$$

$$\bar{N}^{i-} = \left\{(\bar{\rho}^i) - \frac{1}{Bo}\frac{\partial\bar{\rho}^i}{\partial\bar{x}}\right\}_{\bar{x}^-} \tag{7}$$

$$\bar{N}^{i+} = \left\{(\bar{\rho}^i) - \frac{1}{Bo}\frac{\partial\bar{\rho}^i}{\partial\bar{x}}\right\}_{\bar{x}^+} \tag{8}$$

A set of N equations of the form of Eq. (2) and $(N-1)$ equations of the form of Eq. (6) connecting them is obtained. If the number of cells ahead and behind the tracer cell is large, then the concentrations at the end cells should be low, such that the boundaries imposed would be either the Neumann boundary conditions

$$\{\bar{N}^{i-}\}_{k=0} = \left\{(\bar{\rho}^i) - \frac{1}{Bo}\frac{\partial\bar{\rho}^i}{\partial\bar{x}}\right\}_{\bar{x}^-} = 0 \tag{9}$$

$$\{\bar{N}^{i+}\}_{k=N-1} = \left\{(\bar{\rho}^i) - \frac{1}{Bo}\frac{\partial\bar{\rho}^i}{\partial\bar{x}}\right\}_{\bar{x}^+} = 0 \tag{10}$$

or the Dirichlet boundary conditions

$$(\bar{\rho}^i)_{k=0,\bar{x}^-} = 0 \tag{11}$$

$$(\bar{\rho}^i)_{k=N-1,\bar{x}^+} = 0 \tag{12}$$

The model given by Eqs. (2), (6)-(8), (11) and (12) can only be solved numerically. However, for large Bo an analytical expression can be obtained. The asymptotic limit of expression (2) as the Bodenstein number value becomes large is given by Eq. (13). This is the governing equation of a plug flow reactor (PFR). Furthermore, each slug can be considered as a continuous stirred tank reactor (CSTR). Each unit cell appears then as a combination of PFR–CSTR in series. The tracer flux is governed purely by convection in the film and only cells downstream of the initial tracer cell will be affected.

$$\frac{\partial\bar{\rho}^i}{\partial\bar{t}} + \left(\frac{\partial\bar{\rho}^i}{\partial\bar{x}}\right) = 0 \tag{13}$$

The residence time distribution of a PFR–CSTR series is given by [13].

$$E(t) = 0 \quad (t < \tau_p) \tag{14}$$

$$E(t) = \frac{e^{-(t-\tau_p)/\tau_s}}{\tau_s} \quad (t \geq \tau_p) \tag{15}$$

For a cell at the inlet of the reactor with unit concentration that encounters clear liquid at its inlet as it moves, the concentration in the slug is given by Eq. (16)

$$\bar{\rho}(t) = 1 + (e^{-(t-\tau_p)/\tau_s} - 1)\,h(t) \tag{16}$$

where $h(t)$ is the Heaviside unit step function.

Subsequent cell n can be shown to have a slug concentration given by Eq. (17)

$$\bar{\rho}^n(t) = \frac{e^{(t-(n+1)\tau_p)/\tau_s} h(t-(n+1)\tau_p)((t-(n+1)\tau_p)/\tau_s)^n}{\Gamma(n+1)} - \frac{[\Gamma(n) - \Gamma(n,(t-(n+1)\tau_p)/\tau_s)]h(t-(n+1)\tau_p)}{\Gamma(n)} + \frac{[\Gamma(n)-\Gamma(n,(t-n\tau_p)/\tau_s)]h(t-n\tau_p)}{\Gamma(n)} \tag{17}$$

where Γ is the Gamma function.

From the unit cell velocity and geometry, the two parameters τ_p and τ_s can be calculated

$$\tau_p = \frac{L_b}{U_b} \tag{18}$$

$$\tau_s = \frac{\bar{V}/\bar{A}}{U_b} \tag{19}$$

2.1. Numerical solution of the low Bodenstein number model

A finite volume method is used to discretise the set of Eqs. (2) and (6) and the Dirichlet boundary conditions (11) and (12). The solution algorithm uses the exponential spatial discretisation scheme and an implicit time discretisation method. Details of the solution method can be found in Patankar [14]. The liquid slug appears as a finite volume cell of volume equivalent to the liquid slug volume. For the first and last films in the series of cells, the left and right hand boundary conditions can be either a zero flux Neumann or a zero concentration Dirichlet boundary conditions. The solution of the system is independent of which is used provided enough cells on both sides of the tracer cell have been specified. The Dirichlet boundary condition was chosen because it is not conservative, i.e. there will appear a loss of tracer mass from the system if the number of cells ahead or after the tracer cells are insufficient. A mass balance at the end of the simulation serves as a check for the number of cells chosen. The tridiagonal system of algebraic equations is solved at each time step to obtain concentration profiles

in the films and slugs. The simulations start with the tracer cell just inside the reactor.

The concentration of the tracer at the channel outlet determines the simulation time. The dimensionless time at which the first unit cell exits is $\bar{L}_{\text{reactor}} - (N_{\text{A}})\bar{L}_{\text{cell}}$. At each time step, the unit cell exiting and its concentration at the reactor outlet are recorded. The simulations stop when a cell with concentration smaller than a tolerance concentration ($\rho^i < 10^{-6}$) leaves the reactor.

A Matlab® code was written implementing the method outlined above. The correct implementation of the numerical method was verified in a number of ways. The solution of the convection-diffusion Eq. (2) for a single film using this method compared well with an analytical solution [15] for the specific initial and boundary conditions used. In addition, the numerical prediction of the model when the value of the Bodenstein number was set to an arbitrary large value agreed well with the prediction of the analytical solution given by expression (17). The CPU time never exceeded one hour for the largest system when executed on an AMD Athlon™ 1.6 GHz processor.

3. Results

The model is applied to a circular channel reactor with 1 m length and 300 μm diameter, which corresponds to $\bar{L}_{\text{reactor}} = 3333$. An example is given below for a tracer diffusivity typical of a liquid–liquid system, ethanol and air physical properties, combination of bubble and liquid slug lengths and a residence time in reactor (∼7.8 min) such that $Bo = 500$, $Ca = 1 \times 10^{-4}$, $\bar{L}_{\text{b}} = 1.10$, $\bar{L}_{\text{s}} = 1$. For this *Ca* the film thickness is equal to $\bar{\delta} = 0.00249$ [16]. Assuming the geometry of a bubble corresponds to a cylinder with spherical caps, the ratio $\bar{V}/\bar{A}$ is calculated to be 122.6. For the simulation the initial tracer cell is placed with 5 cells ahead and 50 cells behind.

The system is solved and the outlet concentrations are given in Fig. 5. The residence time distribution curve is obtained by normalising the concentration-time graph. The mean and standard deviation of the distribution can be used to calculate the vessel dispersion number (*VDN*) using Eq. (20), [13].

$$\frac{\sigma^2}{t_m^2} = 2(VDN) + 8(VDN)^2 \tag{20}$$

where t_{m} and σ are the mean and standard deviation of the distribution given in Fig. 5. The vessel dispersion number is the non-dimensionalised dispersion coefficient in the dispersion model [13]. In the above example $VDN = 4.92 \times 10^{-6}$.

The effect on the vessel dispersion number of the three non-dimensional numbers, *Ca*, $\bar{L}_{\text{s}}$ and $\bar{L}_{\text{b}}$ that define the geometric characteristics in a Taylor flow system can be seen in Figs. 6 and 7. Both figures show very low *VDN* values, confirming that axial mass transfer in a liquid is significantly reduced with Taylor flow to near PFR level.

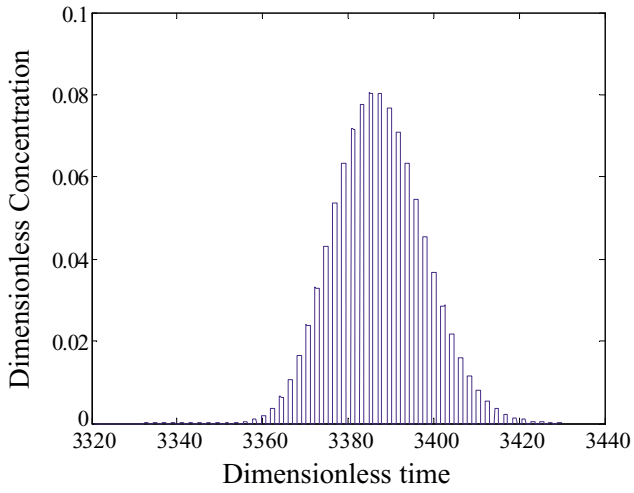

Fig. 5. Concentration of tracer in the liquid slugs exiting the reactor channel. Each peak corresponds to the concentration in an exiting slug. The spacing between the peaks is determined by the length of the liquid film surrounding the bubbles.

For comparison, the vessel dispersion number for laminar flow of liquids in tubes is at least three orders of magnitude larger [13]. An increase in *VDN*, and hence axial mixing, with increasing *Ca* can also be seen. This is to be expected as increased *Ca* results in thicker liquid films that would favour communication between slugs. It can also be seen that *VDN* increases with $\bar{L}_{\text{s}}$ and $\bar{L}_{\text{b}}$. It should be noted that a change in $\bar{L}_{\text{b}}$ does not affect the concentration of the exiting slugs. The increase in the spacing between the different slugs caused by the increased bubble length affects the mean and standard deviation of the residence time distribution as predicted by Eq. (20) and hence *VDN*. For reduced *VDN* in a Taylor flow

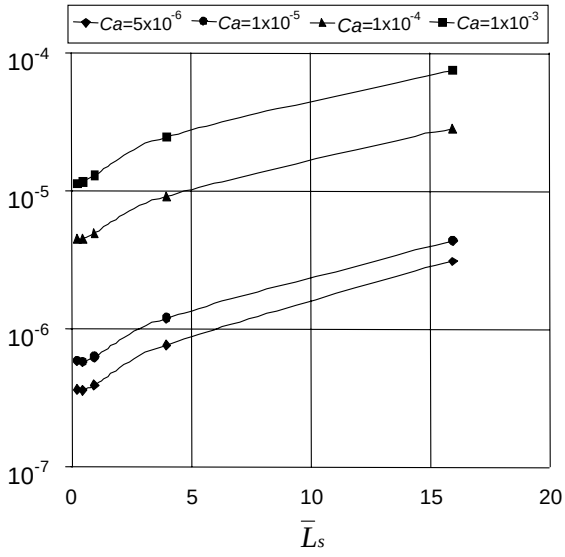

Fig. 6. Variation of the vessel disperion number with $\bar{L}_{\text{s}}$ and *Ca* for a bubble length of $\bar{L}_{\text{b}} = 1.1$.

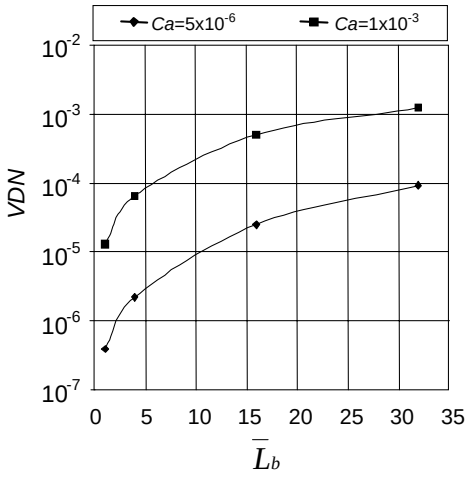

Fig. 7. Variation of the vessel disperion number with bubble length $\bar{L}_b$ and *Ca* for slug length of $\bar{L}_s = 1.0$.

system with mass transfer, short bubble and slug lengths should be formed at the inlet.

Comparison of the results from the numerical technique to the analytical solution given by Eq. (17) showed about 2% difference in predictions for the lowest Bodenstein numbers. Decreasing the Bodenstein number below 10 to a value of 2 showed a much more significant difference in the predictions of the two models. The analytical solution (Eq. (17)) can therefore be used for *Bo* larger than 10.

The simple numerical model described above is suitable for low Bodenstein numbers where diffusion is sufficiently large for mixing to ensure uniform concentration in the slug. To find the upper limit of the Bodenstein number up to which this simple model can be used, results were compared with detailed numerical simulations [12] which incorporate the flow field inside each unit cell. These showed that the present model may be used for *Bo* up to 500, above which the model starts to underpredict the vessel dispersion number.

It is worth noting that the cuves in Figs. 6 and 7 are independent of the Bodenstein number for $10 < Bo < 500$.

Finally, with increasing slug length, the behaviour of the unit slug deviates more and more from being a well mixed region and the time needed for the material to convect and diffuse from one end of the slug to the other would become significant. $\bar{L}_s = 16$ was found to be an upper limit for the above model.

4. Conclusions

A numerical model has been developed for axial mixing in microchannel Taylor flow. The model assumes uniform concentration in the liquid slugs and uses a uniform velocity and concentration in the film surrounding the bubbles. The model can either be solved numerically, or for large Bodenstein numbers, simplified to yield an analytical solution.

The model was found to be suitable for ranges $Ca < 10^{-3}$, $Bo < 500$ and $\bar{L}_s < 16$. Axial mixing was in general very low. Trends show increasing vessel dispersion number (increasing axial mixing) with increasing capillary number and slug and bubble lengths. In addition, for $Bo > 10$, the simple analytical expression was also able to predict axial mixing with small deviations from the numerical model.

Acknowledgements

This work was supported by the EU KEMiCC project G1RD-CT2000-00469.

References

[1] T.C. Thulasidas, M.A. Abraham, R.L. Cerro, Flow patterns in liquid slugs during bubble-train flow inside capillaries, Chem. Eng. Sci. 52 (17) (1997) 2947–2962.
[2] S. Irandoust, B. Andersson, Mass-transfer and liquid-phase reactions in a segmented 2-phase flow monolithic catalyst reactor, Chem. Eng. Sci. 43 (8) (1988) 1983–1988.
[3] S. Irandoust, B. Andersson, Simulation of flow and mass-transfer in Taylor flow through a capillary, Comput. Chem. Eng. 13 (4–5) (1989) 519–526.
[4] G. Bercic, A. Pintar, The role of gas bubbles and liquid slug lengths on mass transport in the Taylor flow through capillaries, Chem. Eng. Sci. 52 (21/22) (1997) 3709–3719.
[5] G. Bercic, Influence of operating conditions on the observed reaction rate in the single channel monolith reactor, Catal. Today 69 (2001) 147–152.
[6] L.J. Skeggs, An automatic method for calorimetric analysis, Am. J. Clin. Pathol. 28 (1957) 311–322.
[7] R.H. Patric, T. Klindera, L.L. Crynes, R.L. Cerro, Residence time distribution in three-phase monolith reactor, AIChE J. 41 (3) (1995) 649–657.
[8] T.C. Thulasidas, M.A. Abraham, R.L. Cerro, Dispersion during bubble-train flow in capillaries, Chem. Eng. Sci. 54 (1999) 61–76.
[9] H. Pedersen, C. Hovarth, Axial dispersion in a segmented gas–liquid flow, Indus. Eng. Chem. Fundam. 20 (1981) 181–186.
[10] R.K. Edvinsson, S. Irandoust, Finite-element analysis of Taylor flow, AIChE J. 42 (7) (1996) 1815–1823.
[11] T.C. Thulasidas, M.A. Abraham, R.L. Cerro, Bubble-Train flow in capillaries of circular and square cross section, Chem. Eng. Sci. 50 (2) (1995) 183–199.
[12] W. Salman, A. Gavriilidis, P. Angeli, Axial Mixing During Taylor Flow in Microchannels, in preparation.
[13] O. Levenspiel, 1990, Chemical Reaction Engeenering, Wiley, New York.
[14] S.V. Patankar, 1980, Numerical Heat Transfer and Fluid Flow, McGraw-Hill.
[15] I. Boztosun, A. Charafi, M. Zerroukat, K. Djidjeli, Thin-plate spline radial basis function scheme for advection-diffusion problems, Electron. J. Boundary Elem. BETEQ 2001 (2) (2002) 267–282.
[16] J.D. Chen, Measuring the film thickness surrounding a bubble inside a capillary, J. Colloid Interf. Sci. 109 (2) (1986) 341–349.